Chapter 9
Coherency Estimation in Power Systems: A Koopman Operator Approach

Harold R. Chamorro, Camilo A. Ordonez, Jimmy C.-H. Peng, Francisco Gonzalez-Longatt and Vijay K. Sood

Abstract Integrating a significant amount of non-synchronous generation into power systems creates new technical challenges for transmission systems. The research and understanding of the impact of the non-synchronous generation through back-to-back Full Rated Converters' (FRCs) on power system's coherency is a matter of importance. Coherency behavior under the presence of large inclusion of non-synchronous generation requires more research, in order to understand the forming groups, after a disturbance, when the inertia is decreasing due to the decoupling. This document presents the application of the so-called *Koopman Operator* for the identification of coherent groups in power systems with the influence of non-synchronous generation. The *Koopman* Analysis clusters the coherent groups based on the measurements obtained. The visualization of the coherent groups identified allows to observe their dynamic variations according to the penetration level or fault location. The applied method of coherency identification is evaluated in the Nordic test system through gradually increasing integration of non-synchronous generations and different fault scenarios.

H. R. Chamorro (✉)
KTH Royal Institute of Technology, Teknikringen 33, Stockholm, Sweden
e-mail: hrcv@kth.se; hr.chamo@ieee.org

C. A. Ordonez
Grupo Energia Bogota, Carrera 9 # 73-44, Bogotá, Colombia
e-mail: cordonezm@geb.com.co

J. C.-H. Peng
National University of Singapore, Singapore, Singapore
e-mail: elepcj@nus.edu.sg

F. Gonzalez-Longatt
Loughborough University, Holywell Park, Epinal Way, Loughborough, UK
e-mail: f.gonzalez-longatt@lboro.ac.uk

V. K. Sood
University of Ontario Institute of Technology, Oshawa, ON L1H 7K4, Canada
e-mail: vijay.sood@uoit.ca

M. J. Blondin et al. (eds.), *Computational Intelligence and Optimization Methods for Control Engineering*, Springer Optimization and Its Applications 150,
https://doi.org/10.1007/978-3-030-25446-9_9

9.1 Introduction

The considerable environmental benefits of integrating renewable generation into the grid have encouraged several governmental policies around to world. Since the non-synchronous generation (wind, wave and solar power) is required to behave like conventional synchronous generation units, (full-scale power supply) the high voltage power electronics converters have become attractive to be selected for the integration into either the transmission or distribution power levels [1].

A wider use of non-synchronous generation relies on the use of Full Rated Converters (FRCs). This is due to them enabling multiple control features which include controlling active and reactive power [2], assuring voltage ride through capability [3] in order to deal with variable speed wind turbines [4], and adding Maximum Power Point Tracking (MPPT) algorithms [5]. However, the generation is completely decoupled from the system, and is consequently unable to contribute dynamically to the system [6, 7]. Thus, if the synthetic inertia control option is not added, the decoupling displaces synchronous machines [8].

The reduction of the inertia in the power grid has provoked a global concern by the system operators, power planners and researchers. Several reports have shown the experience with large inclusion of non-synchronous generation and the dynamical challenges during the past years [9].

Some of the main challenges which have been reported include the following:

- The first experienced challenge is the decrease in the system inertial response which affects the dynamical response [10–12].
- The second challenge due to non-synchronous integration is the impact on small signal stability. Several studies have shown that the large-scale inclusion of wind power degrades the damping of the electromechanical modes. This displace them to a different stability operation region, thereby affecting the response of the system under small and large disturbances [13, 14].

A study conducted in [15] analyses the impact of the effect of high penetration of photovoltaic (PV) on small signal stability. Due to the reduced system inertia the study result showed a reduction in the damping torques of the system. A transient and small signal stability analyses with a gradual inclusion of PV are developed in [16], the eigenvalue results show that a displacement of conventional units have a great impact on the oscillatory modes.

- The third challenge is the coherency of power systems and how it can be affected by the use of high power electronic converters. One relevant study shows that the large-scale inclusion of wind power changes the coherency of the synchronous generators coherent groups [17], however additional research is required in understanding how the non-synchronous generation affects the coherency in power systems.

The phenomenon of coherency in large interconnected power systems is presented when some generators swing together after a disturbance [18, 19]. To identify coherent groups, different methods have been studied during the last years in literature.

Time and frequency-domain methods have been used to analyse the coherency of generators [20, 21]. Partitioning-based slow coherency methods have been presented in [22, 23].

Support vector clustering is applied for coherency studies in [24], computing compact and separated clusters based on the measurements obtained.

Some approaches applying machine learning and computational intelligence techniques for coherent identification have also been investigated in [25, 26]. In [27], neural networks, as patterns recognition and classificators sets are used. In a more recent contribution [28], where neural networks are also used, a fast method for security assessment is proposed. Fuzzy clustering methods have also been applied in [29] and [30] with auto-configuring training, and c-means clustering methods, respectively.

Another related method is presented in [31], which applies maximum spanning tree partitioning, to obtain the strongest connections in the network after a disturbance.

One method is developed in [32], where the flocking agent-interaction method is applied for different scenarios including rapid clustering identification.

Digital signal processing techniques have been applied in this topic. One important contribution is presented in [33], where the wavelet transform is used to obtain the phase relations according to the signals, and is used to determine the common frequencies of the generators involved. Another important approach is given in [34], where the Hilbert-Huang transform is tracking the generator coherency instantaneously.

Coherency-based graph theory has been studied in [35] and [36], where the topological network structure is analysed. In this method the generators are clustered according to the sub-networks and cut-sets obtained.

In [17], the coherency including wind farms is studied. The determination of the coherent groups is done by the rotor angle response observation after a fault.

The *Koopman operator* has proven to be a suitable method for coherency identification in power systems [37]. Koopman Mode Analysis (KMA) provides a graphical tool based on linear transformations on Hilbert spaces to analyse (non-linear) Hamiltonian systems. This linear, infinite-dimensional operator is defined for any non-linear dynamical system [38, 39]. One important characteristic of the Koopman operator is its ability to capture the full pattern information of large complex dynamical systems like power grids. Also, in [40], an islanding method is proposed and it is shown that the Koopman operator can determine the static connectivity of a system in a similar way as graph theory does.

This document follows the theory presented in [41], and also applies the technique developed in [37] and [42]. Otherwise, the same mentioned authors, in a most recent contribution of KMA presented in [43], the authors show the application in the 2006 European Grid-wide disturbance [44]. It is demonstrated the versatility of the KMA by decomposing the power exchanges between the operative areas in order to not only observe the coupled swing dynamics, but use the KMA to diagnose the instabilities using the data obtained from a real past case [43].

The main contributions of this document are the follow ones. The first one, is the coherent groups identification including non-synchronous generations in power systems which has been barely studied in literature before, and second one, to address the notion of how the reduction of inertia by the large penetration of power converters change affects the coherency in power systems from the data. Note the Koopman Analysis requires only the measurements of the system, not the model, which makes a robust and practical graphical tool. Moreover, the analysis is illustrated in a test system under the consideration of different penetration level scenarios and fault locations illustrating gradually the coherent groups conformation.

This document is an extended version of [2, 70] and is structured as follows. In Section 9.2, the problem formulation of coherency identification in non-synchronous integration is presented. In Section 9.3, the preliminaries of the theory of the *Koopman operator*, the definition of KM and the coherency definition are reviewed. In Section 9.4, the coherency in the Nordic test system is studied under different faults. Section 9.5 presents the case studies regarding the gradual increasing of non-synchronous generation integration on the test system. Finally, the conclusions and future work of this research are given.

9.2 Problem Formulation

The identification of coherent groups is of importance for the development, deployment and implementation of control schemes to improve the system transmission capability [45]. Having identified coherent groups, it is possible to classify those generators that are oscillating together, in order to understand the dynamic behaviour of the system under disturbances, and design appropriate controllers to protect it against them [46].

Coherency identification can be used in Wide Area Monitoring Protection and Control (WAMPAC) systems [47] in different ways. For instance, controlled islanding uses the coherency identification to know how to split the network into different sub-groups, and to avoid a blackout of the complete system [48, 49].

A dynamic preventive observation of the coherent groups can confine cascading faults within smaller self-sustainable islands making the grid more robust under disturbances [50].

Self-healing schemes can also be improved through the observation of the coherent groups to protect, apply control actions and restore the system after a fault [51].

The identification of coherent groups can also be helpful to locate, design or tune Power System Stabilizers (PSS) [52, 53]. Furthermore, the design of Flexible AC Transmission Systems (FACTS) controllers can also take advantage of the coherent groups identification as shown in [54], where the feedback measurements are selected based on the dominant machines of the identified groups.

Moreover, cyber-security schemes can take advantage of the coherent identification as a tool for monitoring the dynamic changes instantaneously and upgrade the control decisions faster [55, 56]. Furthermore, it is possible to propose dynamic security assessments to make the response of the protection systems more efficient

and adaptable, and also to conceive advanced alert systems in order to avoid large area disturbances [57, 58].

Coherency identification methods can be classified into two basic groups [59]. The first one is based on linearised models of power systems [60, 61]. These methods might not be completely suitable since they do not capture the post-fault dynamics. The second group can be called measurement-based methods, because they rely on the signals obtained from the system, either off-line or on-line methods, to bring a more precise dynamic observation of the system [62].

9.2.1 Koopman Self-clustering Optimization

One of the biggest concerns in Wide Area Measurement Systems (WAMS) is the effective computing techniques and measurement technologies which allow to visualize the dynamics of the systems and use the data for short/long term power system planning [63, 64]. Koopman Mode Analysis (KMA), in its current stage of development, is capable of receiving the signals from simulation or measured data, providing the clusters of the coherent groups. Certainly, the method has the potential to be a real-time coherency method; but further research is needed. Otherwise, the computational effort of the analysis is based only in the mathematical (numerical) calculation which can be carried out by any of the processors developed in the current technological age, or it can be easily embedded in a Hardware in-the-Loop (HiL) system or even a Floating Point Gate Array (FPGA). However, these two latest aspects are not the purpose of this document.

The visualization of the method also plays an important role, e.g. from the Transmission System Operator (TSO) point of view. The display of the results should be easy to understand by the operator, who is responsible for planning the interconnection of HVDC lines or large non-synchronous generation, and determine decisions on-time, propose control strategies to prevent undesirable events, etc. The results, and the final results display obtained by the use of the KMA (phase vs. amplitude diagrams), can bring a friendly interpretation of the dynamics variations in the power systems supervised.

One of the main robust characteristic of KMA is that can handle several data (e.g from data-receivers or predicted models) providing an assessment for short/long-term futuristic power planing and update the control systems based on the analysis given [43].

Partitioning power networks (islanding) for protecting the grid of blackouts and large collapses using KMA has an important advantage, the model-free and the relying on dynamics data in the network [40].

Coherency identification using KMA belongs to the measurement-based group since it only requires sampled data [65]. Apart of the mentioned advantages, KMA has some important characteristics which makes it a powerful tool. The first, and most important one is that it deals with non-linear dynamics. Secondly, it does not need

any training process, such as neural networks or support vector machines, because this method lies on the spectrum calculation of the Koopman Operator.

The aim of this paper is to show that the KMA can be used for identification of coherent swings and generators in systems under the effect of the decoupling of full converters. In this paper, non-synchronous generation is modelled by aggregated full converter units with the same power rating as that of the replaced synchronous generation.

9.3 Koopman Operator Preliminaries

9.3.1 Koopman Operator, Eigenvalue and Mode

Consider the following dynamics described by a discrete-time non-linear system evolving on a smooth manifold [40, 66].

$$x_{k+1} = F(x_k) \tag{9.1}$$

where, $x_k \in M$ is the state variable belonging to state space M, and $F : M \to M$ is a non-linear, vector-valued function. The *Koopman Operator* is a linear operator $\mathscr{U}$ that acts on scalar-values functions on M in the following manner: for $g : M \to \mathbb{R}$, $\mathscr{U}$ maps g into a new function $\mathscr{U}g$ given by

$$\mathscr{U}g(x) = g(F(x))$$

Although the dynamical system is non-linear and evolves on a finite-dimensional space, the *Koopman operator* is linear, but infinite-dimensional. The *Koopman eigenfunctions* $\varphi_j : M \to \mathbb{C}$ and the *Koopman eigenvalues* (KEs) $\lambda_j \in \mathbb{C}$ associated to $\mathscr{U}$, are defined as

$$\mathscr{U}\varphi_j(x) = \lambda_j \varphi_j(x), \qquad j = 1, 2, \ldots$$

Consider $g : M \to \mathbb{R}^p$ a vector-valued observable. If each g_i of the components in $\boldsymbol{g}$ lies within the span of eigenfunction φ_j, then the time-evolution of observable $\boldsymbol{g}(\boldsymbol{x}_k)$ from $\boldsymbol{g}(\boldsymbol{x}_0)$ is expanded as follows:

$$\boldsymbol{g}(\boldsymbol{x}_k) = \sum_{j=1}^{\infty} U^k \varphi_j(\boldsymbol{x}_0)\, \boldsymbol{v}_j = \sum_{j=1}^{\infty} \lambda_j^k \varphi_j(\boldsymbol{x}_0)\, \boldsymbol{v}_j \tag{9.2}$$

where, $\boldsymbol{v}_j$ is the vector-valued coefficient of the decomposition and is called the j-th Koopman Mode (KM) [67]. This decomposition is based on the properties of the point spectrum of U, and the analysis based on (9.2) is called Koopman Mode Analysis (KMA). The KMA enables the extraction of single-frequency modes from

data on fully non-linear dynamics from the temporal behaviour of the corresponding KM. The phase of λ_j determines its frequency, and the magnitude determines the growth rate.

The computation of Koopman eigenvalues and KMs is effectuated by a modified version of *Arnoldi* algorithm described in [68], where it is shown that the *Ritz* value $\tilde{\lambda}_j$ and vector $\tilde{v}_j$ approximate the Koopman eigenvalue λ_j and factor $\varphi_j(\boldsymbol{x}_0)\boldsymbol{v}_j$ in the expansion in terms of a finite truncation.

The input of the algorithm is the $N+1$ sampled data $\{\boldsymbol{g}(\boldsymbol{x}_0), \boldsymbol{g}(\boldsymbol{x}_1), \ldots, \boldsymbol{g}(\boldsymbol{x}_N)\}$. The outputs are N pairs of Koopman eigenvalues and KMs. The finite sum expansion is expressed by:

$$\begin{cases} \boldsymbol{g}(\boldsymbol{x}_k) = & \sum_{j=1}^{N} \tilde{\lambda}_j^k \tilde{\boldsymbol{v}_j} \quad k = 0, \ldots, N-1 \\ \boldsymbol{g}(\boldsymbol{x}_N) = & \sum_{j=1}^{N} \tilde{\lambda}_j^N \tilde{\boldsymbol{v}_j} + \boldsymbol{r} \end{cases} \tag{9.3}$$

where, $\boldsymbol{r}$ is a residue with the approximation error.

9.3.2 Coherency in the Koopman Mode

By denoting $\tilde{v}_{ji}$ as the i-th element of $\boldsymbol{v_j}$, a coherent group of KMs is identified based on the amplitude coefficient $A_{ji} := \mid \tilde{v}_{ji} \mid$ and the initial phase $\alpha_{ji} := arg(\tilde{v}_{ji})$ for each mode j and observable i (e.g. rotor angle δ_i and voltage angle θ_i).

Coherency for KMs is defined in [51] as follows. For given finite N modes $\{\tilde{v}_1, \ldots, \tilde{v}_N\}$ and fixed constants $(\varepsilon_1, \varepsilon_2)$, two observables $\{g_k, g_v\}$ are called $(\varepsilon_1, \varepsilon_2)$-coherent with respect to mode j if

$$\begin{cases} \mid A_{j,k} - A_{j,v} \mid & < \varepsilon_1 \\ \mid \alpha_{j,k} - \alpha_{j,v} \mid & < \varepsilon_2 \end{cases}$$

In this case, $\boldsymbol{g}(\boldsymbol{x}_k)$ contains swing dynamics of synchronous machines in a power system, so it is possible to group the oscillatory components with similar amplitude A_{ji} and initial phase α_{ji} of machines to state them as coherent. This is illustrated in the Figure 9.1.

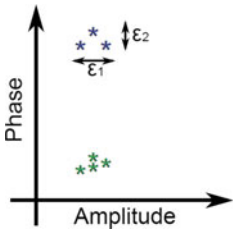

Fig. 9.1 Groups of $(\varepsilon_1, \varepsilon_2)$-coherent observables illustrated in a phase versus amplitude plot

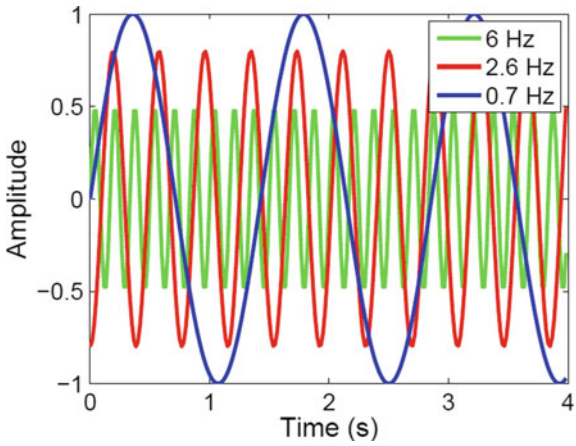

Fig. 9.2 Three sine waves of different frequency corresponding to (9.4). The 2.6 Hz sine wave is displaced by a $\pi/2$ rads phase shift

9.3.3 *Illustrative Example*

Let us consider a simple example of KMA. The signals shown in Figure 9.2 represent the measurements obtained from an oscillatory signal. Notice these signals are not coupled.

$$\begin{aligned} g_1 &= 0.5 sin\,(2\pi f_1 t) \\ g_2 &= 0.8 sin\,(2\pi f_2 t - \pi/2) \\ g_3 &= sin\,(2\pi f_3 t) \end{aligned} \tag{9.4}$$

Here f_1, f_2, and f_3, are chosen as 6, 2.6, 0.7 Hz respectively. These signals are depicted in Figure 9.2 over a time period of 4 s.

Now, KMA is applied with a sampling frequency of $f_s = 60$ Hz to the data. $N + 1 = 240$ samples are acquired giving $N = 239$ modes. The modes are now listed based on the Growth Rate (GR) which is related to the damping in case of sampled dynamics. The five modes with the largest GRs are listed in Table 9.1.

In this manner, the sampled data has been decomposed into a set of $Ritz$ values $\tilde{\lambda}$ and vectors $\boldsymbol{v}$. The dominant frequencies are identified by applying KMA to the

Table 9.1 Dominant $Koopman$ modes obtained for the data shown in Figure 9.2

Mode j	Growth rate	Frequency (Hz)	Norm $\|\tilde{v_j}\|$
1	0.9997	0.68	0.0269
2	0.9960	2.66	0.2814
3	0.9951	5.94	0.0266
4	0.9925	0.39	0.5401
5	0.9913	0.13	0.1816

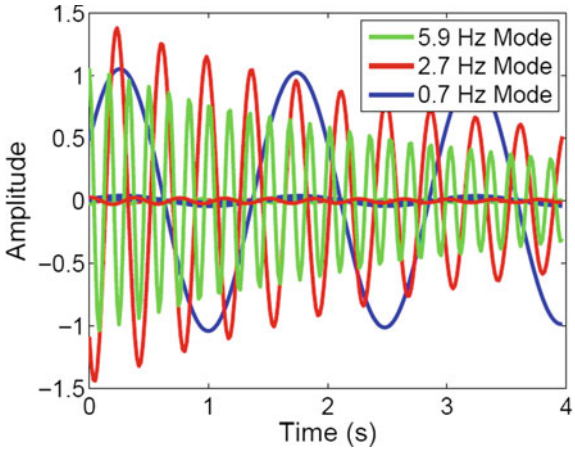

Fig. 9.3 The modal "dynamics" of the three dominant modes. Each of the modes has three contributions corresponding to the three measured observables (the sine waves g_1, g_2, g_3)

sampled data. Modal dynamics for Modes 1-3 are depicted in Figure 9.3. It is seen that for each mode, essentially only one observable (out of three) contributes (the one corresponding to the sine wave of the same frequency as the mode). The sum over all modes according to (9.2)–(9.3) reconstructs the sampled data.

9.4 Application to the Nordic System

The single-line diagram of the Nordic test system is shown in Figure 9.4. This system contains 32 high voltage buses, 20 synchronous generators with different types of generation (circled in the figure), in four geographical identified area. The $North$ and $External$ area are hydro-dominated while the south and central areas have a mixture of nuclear, thermal and coal power plants. Central area has the highest level consumption whereas the North area has the lowest level. The transmission system is designed for 400 kV (19 buses) with some regional systems at 220 kV (2 buses) and 130 kV (11 buses). The details of the system, such as unit rating, line data, dynamic data, and loading conditions, are given in [69]. Power System Stabilizers (PSS) have been located in the following synchronous machines: 1042, 1043, 4011, 4042, 4047, 4051, 4062, 4063.

9.4.1 Numerical Simulation

The setting of numerical simulation is as follows. The constants and power loads are the same as in [69]. All numerical simulations discussed in this paper are performed using the software DigSilent Power Factory®. Then, some disturbances (three-phase

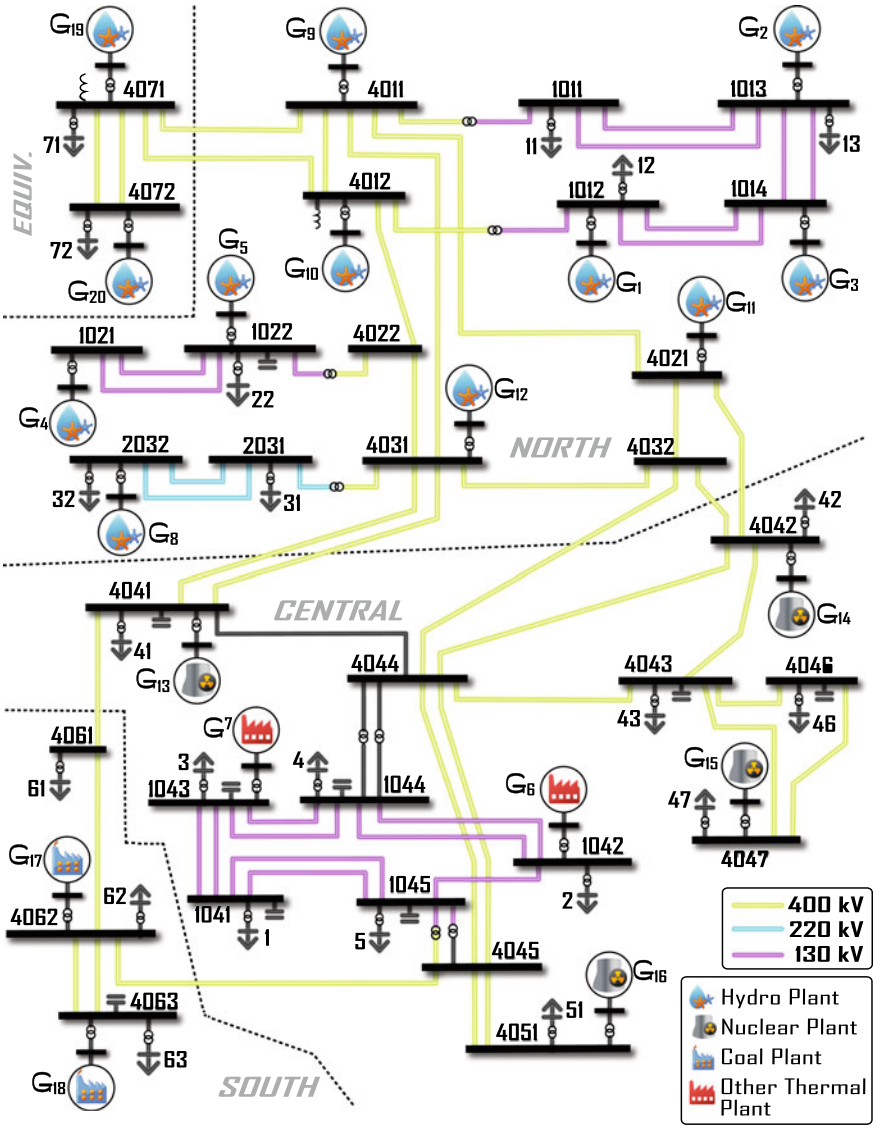

Fig. 9.4 Nordic 32 test system

Table 9.2 List of selected faults—Nordic 32-bus test system

Fault	Bus fault location	Critical clearing time (ms)
1	4047	234
2	1021	190
3	4031	180
4	4063	250
5	1012	250

short circuit faults) in the system are supposed in order to trigger the swing curves signals to analyse. The location of the faults are based on the previous study of this system presented in [70], however the Critical Clearing Time (CCT) differs due to the different dynamic settings in the system (Table 9.2).

9.4.2 Koopman Modes and Eigenvalues Analysis

KM have been computed based on the measurements obtained, which are the rotor angle δ_i of the synchronous generators. For computation, the observable $\boldsymbol{g}(\delta)$ is chosen, where $\delta = [\delta_1, \ldots, \delta_7, \delta_9, \ldots, \delta_{20}]^T$. The symbol T indicates transpose in vectors. It is used on the simulation outputs obtained from the software, where the uniform sampling period $T_s = 1/(f_s)$, with $f_s = 100$ Hz and the number of samples $N = 1001$. An appropriate number of samples should be selected to capture a large quantity enough of snapshots.

Consider a fault located in the bus number B_{4047} located in the $Central$ area. Figure 9.5 shows the time response of the $\Delta\delta_i$. Note that G_8 (G_{4011}) is the reference machine.

The coherent generators extraction are obtained from the KMs decomposition. In this document, the mode of interest is the one with the largest norm. The frequency related to this mode is 0.6Hz. Table 9.3 shows the numerical computation of KEs and KMs, Mode 1 to Mode 10.

The distribution of $A_{8,i}$ versus $\alpha_{8,i}$ is plotted in Figure 9.5. The circle points for generators show the different cluster groups obtained. For this mode, the phase $\alpha_{8,i}$ clusters two main generator coherent groups CG_1 (1012, 1013, 1014, 4012, 4071, 4072) and CG_2 ($G_{1043}, G_{4041}, G_{4042}, G_{4047}, G_{4051}, G_{1042}, G_{4062}, G_{4063}, G_{2032}, G_{4021}$, G_{4031}, G_{1021} and G_{1022}) and different subgroups. Figure 9.6 show the time response of these sub-groups respectively. Observing CG_1 and CG_2 groups and the time response is possible to match which groups have positive and negative rotor angle, or in other words, the accelerating and de-accelerating groups respectively.

Following the same process, it is possible to identify the coherent groups/ subgroups with the different faults stated above. Table 9.4 shows the correspond-

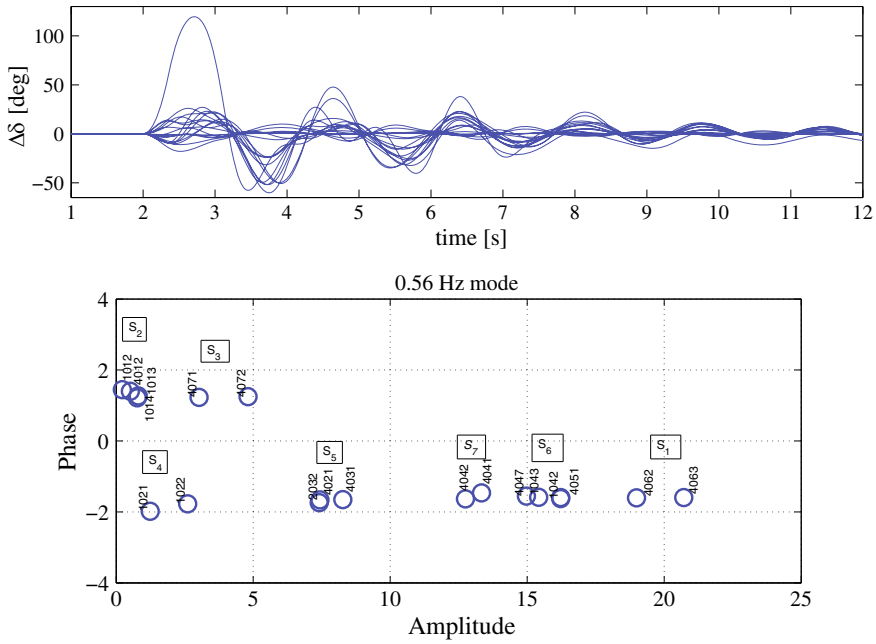

Fig. 9.5 Rotor angle time response after the fault at bus B_{4047}

Table 9.3 Result of *Koopman* modes after fault in B4047

Mode j	Growth rate	Frequency (Hz)	Norm $\|\tilde{v_j}\|$
1	1	0	115.9
2	0.9987	1.8169	0.20029
3	0.99844	2.049	0.11828
4	0.9983	2.1693	0.10667
5	0.9982	1.9336	0.18931
6	0.99809	1.6843	0.42954
7	0.99796	2.2854	0.11777
8	0.99748	0.59578	73.438
9	0.99746	0.2983	2.3481
10	0.99745	1.3594	1.6117

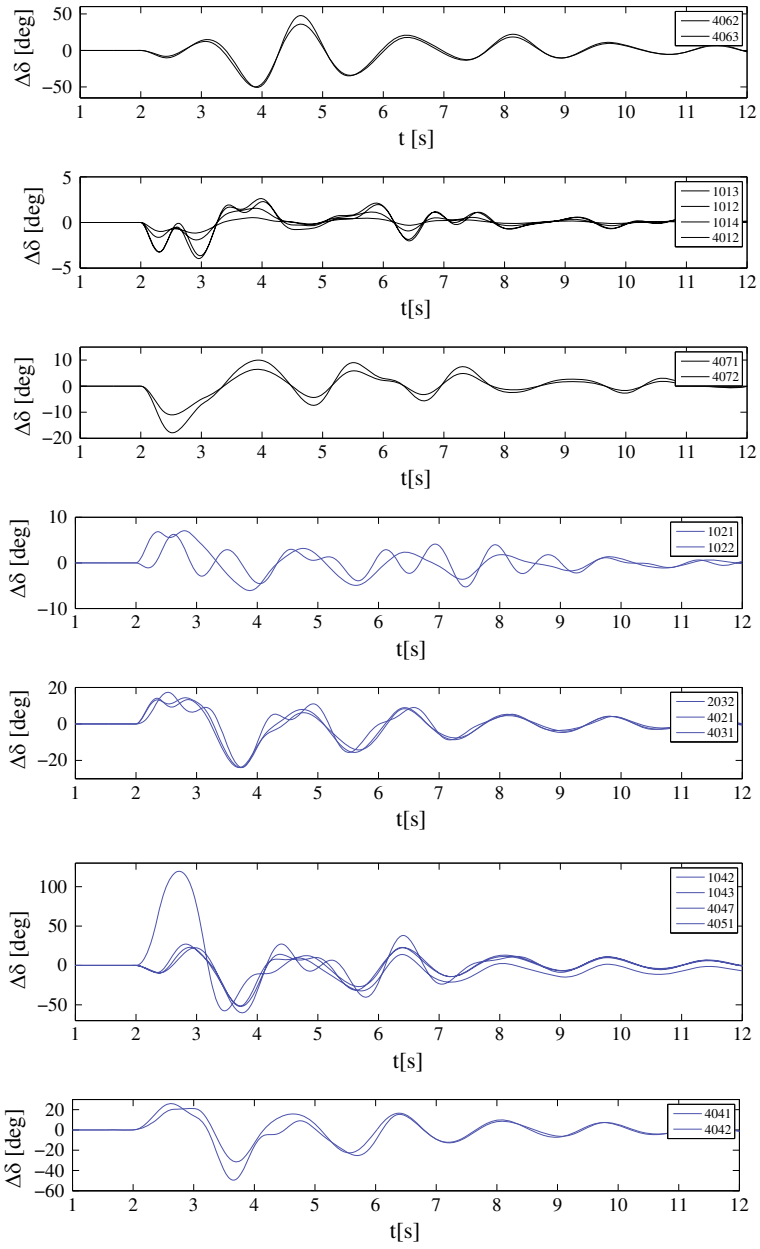

Fig. 9.6 Coherent sub-groups identified after the fault at bus B_{4047}

Table 9.4 Largest Koopman modes for the different faults

Fault	Mode j	Growth rate	Frequency (Hz)	Norm $\|\tilde{v_j}\|$
4031	3	0.99797	0.616	60.08
1021	2	0.99108	0.569	8.539
4063	8	0.99748	0.595	73.43
1012	3	0.99798	0.613	78.68

ing KMs and their frequencies according to the rest of the faults. Figure 9.7a–d show the distribution of the largest Koopman Modes.

Same groups ($CG_1$and CG_2) and subgroups are obtained, nevertheless some slightly differences can be observed. For the fault located in bus B_{4063}, it can be seen in Figure 9.7c that G_{4062} and G_{4063} are more related to the central group of generators than other cases. Sub-group S_7 can be joined with sub-group S_6. The other generators remained to the same sub-groups.

9.5 Test Cases: Gradual Increasing of Non-synchronous Generation

The impact of the integration of non-synchronous generation on the test system coherency is analysed by replacing some of the synchronous generators with back-to-back FRC with the same active and reactive power outputs in order to guarantee the same initial conditions. Note that the power outputs are fixed through the simulation. Two scenarios are tested: first one, replaces synchronous generators in the Central-South area while the second one replaces in the North-External area.

9.5.1 Scenario Central-South

Case 1 (C_1) to Case 5 (C_5) represent the replacement of synchronous generation by the integration of non-synchronous generation based FRC gradually, in order to analyse different levels of power penetration. For example, C_1 considers the replacement of one generation only, and C_2 considers the replacement of two generators including the one in C_1, and so on. It is assumed that the dispersed generation is connected to one established substation. These five scenarios are summarised in Table 9.5:

Initially, KM are evaluated for fault at B_{4047} for cases presented above. Table 9.6 shows the KM variation according to the replacement by non-synchronous in the system. It can be seen that the largest mode frequency stays in the same range. The same behaviour is obtained in the rest of the cases; however, the frequency tables variation are not presented here.

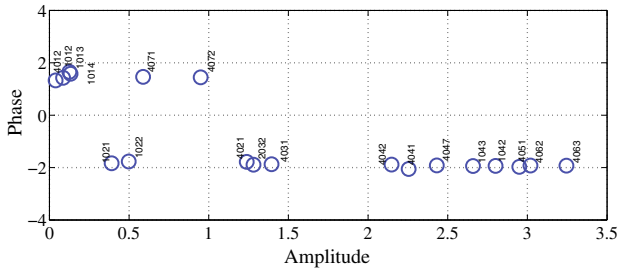

(a) Distribution of initial phases α_{ji} and amplitude coefficients A_{ji} (after fault at bus B_{1021})

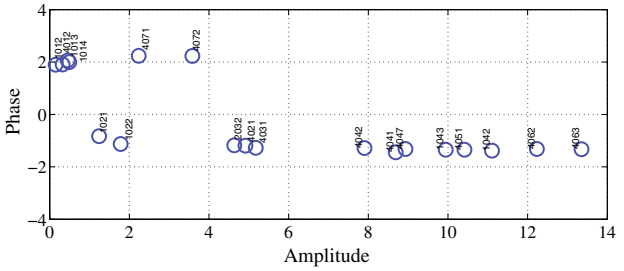

(b) Distribution of initial phases α_{ji} and amplitude coefficients A_{ji} (after fault at bus B_{4031})

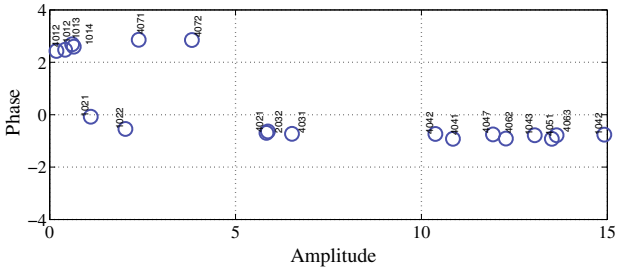

(c) Distribution of initial phases α_{ji} and amplitude coefficients A_{ji} (after fault at bus B_{4063})

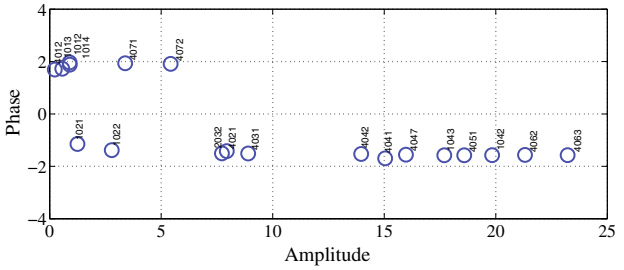

(d) Distribution of initial phases α_{ji} and amplitude coefficients A_{ji} (after fault at bus B_{1012})

Fig. 9.7 Distribution of initial phases and amplitude coefficients for different faults

Table 9.5 Generator replacement for each case

Case	C_1	C_2	C_3	C_4	C_5
Generator	G_7	G_{16}	G_{17}	G_{14}	G_6
Bus	B_{1043}	B_{4051}	B_{4062}	B_{4042}	B_{1042}
Power (MW)%	1.2	5.4	9	13	15

Table 9.6 Koopman largest mode variation (fault 4047)

Mode j	Growth rate	Frequency (Hz)	Norm $\|\tilde{v_j}\|$	Case
8	0.99748	0.5957	73.43	BC
15	0.99721	0.5908	75.54	C_1
3	0.99894	0.5714	52.31	C_2
6	0.99813	0.5661	19.23	C_3
10	0.99789	0.5986	22.17	C_4
4	0.99978	0.6542	9.365	C_5

KM for C_2 is plotted in Figure 9.8. The replacement by non-synchronous generation in the first two cases does not affect the coherent groups/sub-groups analysed before. Figure 9.8 shows the KM for C_3 and the significant changes for cases C_4 and C_5 with the circle points variation of the generators concerned. After the third case, with the replacement of generator G_{4062}, generator G_{4063} (both in the South area) become to swing and be more coherent with generators in the Central area. Generators in the $North$ and $External$ area keep swinging together.

For the fault in bus B_{4031}, first two cases of non-synchronous generation replacement do not show change in the coherent sub-groups as the former analysis. From the third case, significant changes can be observed in the KM sub-groups. The sub-groups based on the amplitude coefficient of the respective mode show that the Central area have become more separated. Specially in case 4, where generator G_{1042} moves closer to G_{4063} (Figure 9.9).

Generator G_{1042} is becoming more separate in C_4 for post-faults in buses B_{4063}, B_{4012} and B_{4021} as it can be seen in Figures 9.10 and 9.11 (Figure 9.12).

9.5.2 Scenario North-External Area

This scenario considers the replacement of some generators in the North and External area. The location of these new cases in the system are presented in Table 9.7. It is applied the same gradual replacement from the previous scenario.

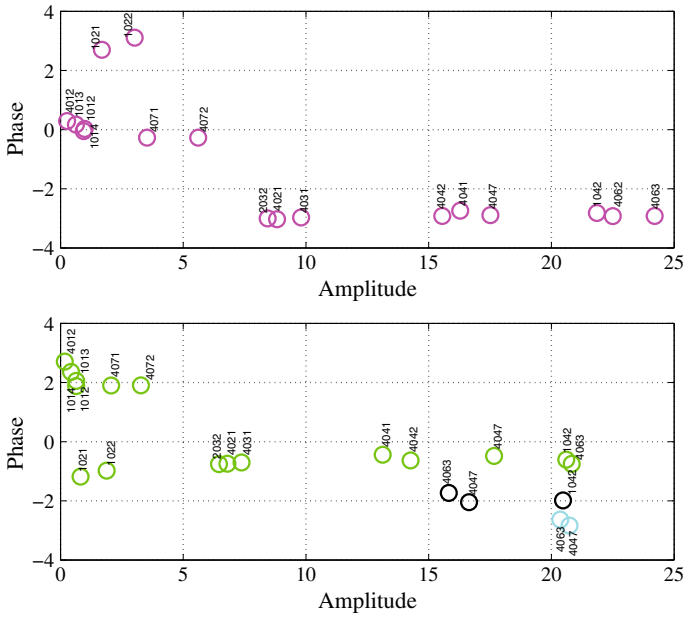

Fig. 9.8 Coherency identification including non-synchronous generation (after fault at bus B_{4047})

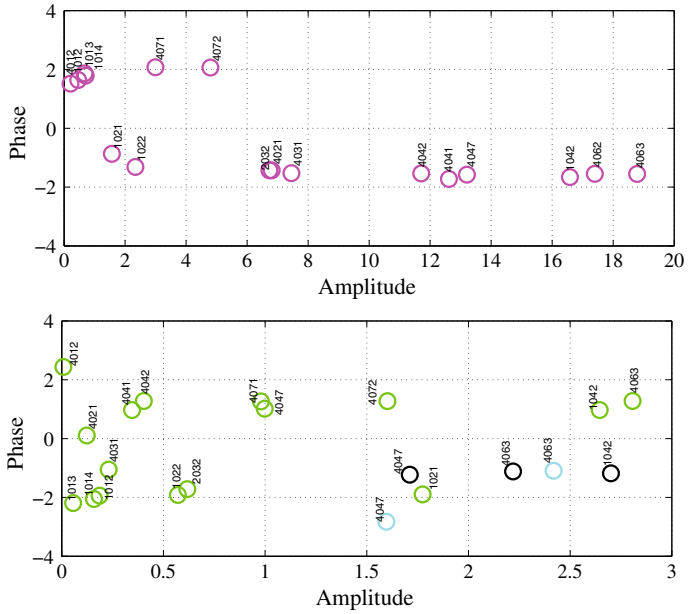

Fig. 9.9 Coherency identification including non-synchronous generation (after fault at bus B_{4031})

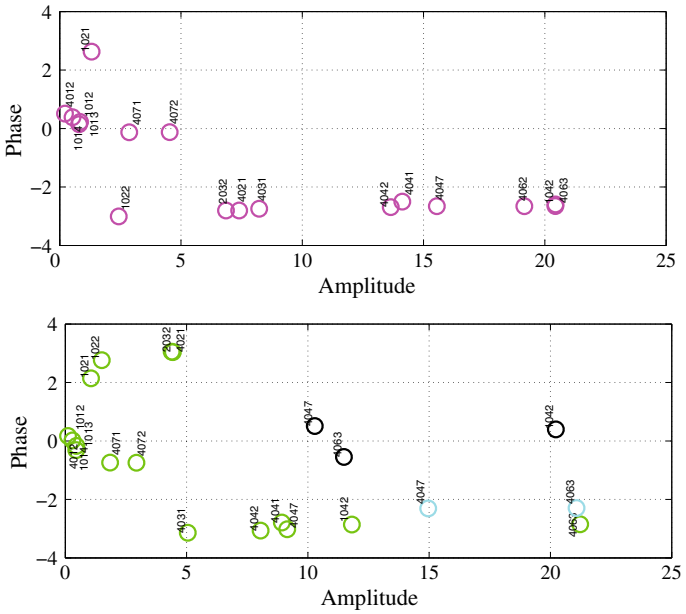

Fig. 9.10 Coherency identification including non-synchronous generation (after fault at bus B_{4063})

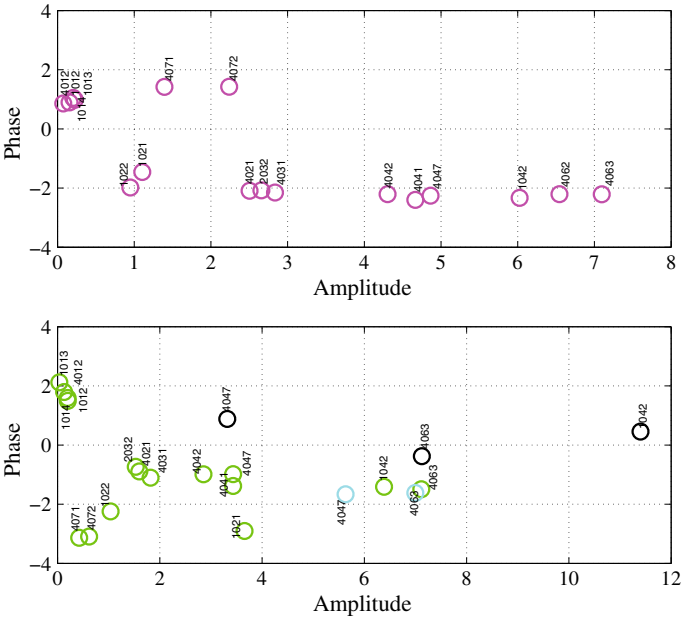

Fig. 9.11 Coherency identification including non-synchronous generation (after fault at bus B_{1021})

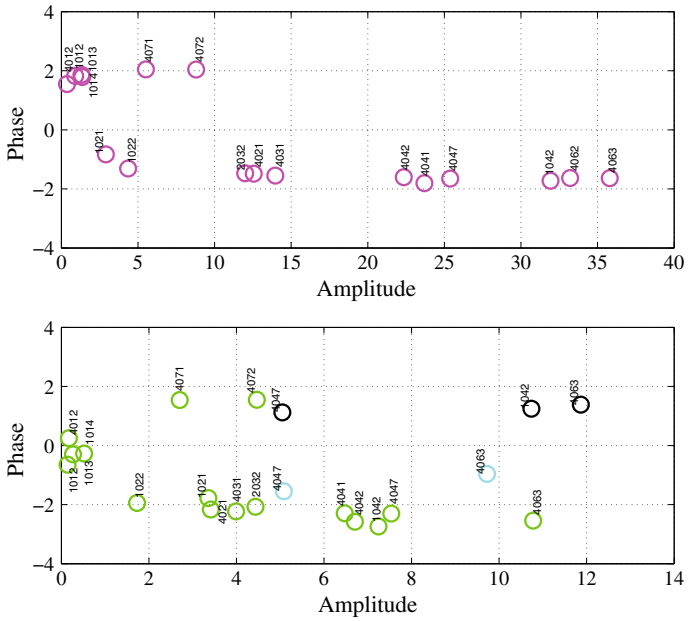

Fig. 9.12 Coherency identification including non-synchronous generation (after fault at bus B_{1012})

Table 9.7 Generator replacement for each case (North-Ext)

Case	C_1	C_2	C_3
Generator	G_2	G_{12}	G_{19}
Bus	B_{1013}	B_{1012}	B_{4071}
Power (MW)%	3	6	9

The replacement by non-synchronous generation in the first two cases remains the sub-groups previously identified for the same faults located. After the replacement of the third generator, for the fault located in bus B_{4031}, makes the generator G_{1021} be more coherent with the sub-group of generators G_{4012} and G_{1014}, whereas for the faults located in buses B_{1021} and B_{1012} the generator G_{1021} be more coherent with the generators G_{2032}, G_{4031} and G_{4021}. This is shown in Figures 9.13, 9.14 and 9.15 (Table 9.8).

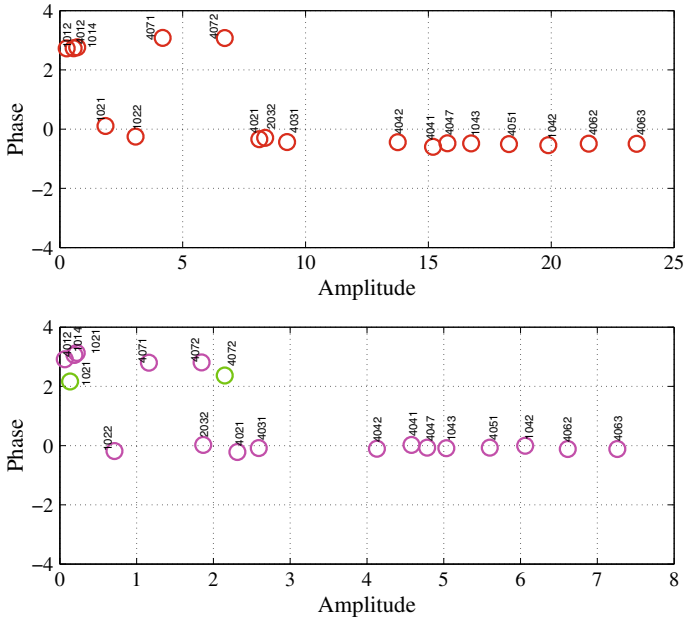

Fig. 9.13 Coherency identification including non-synchronous generation (after fault at bus B_{4031})

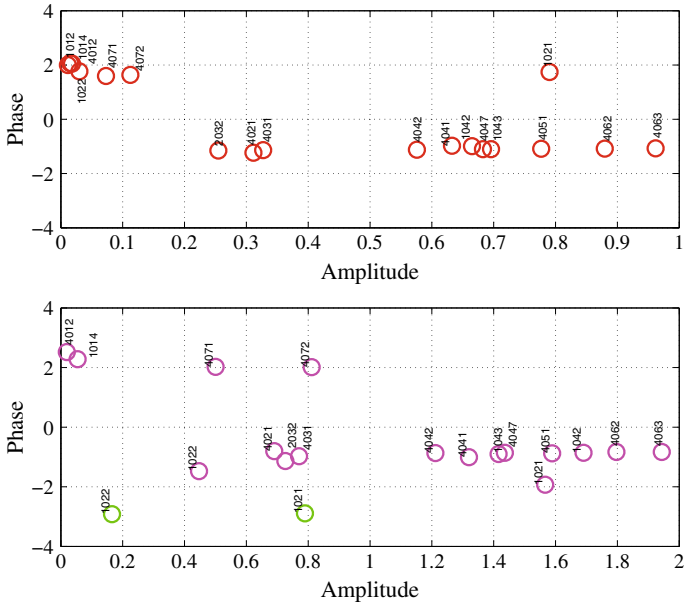

Fig. 9.14 Coherency identification including non-synchronous generation (after fault at bus B_{1021})

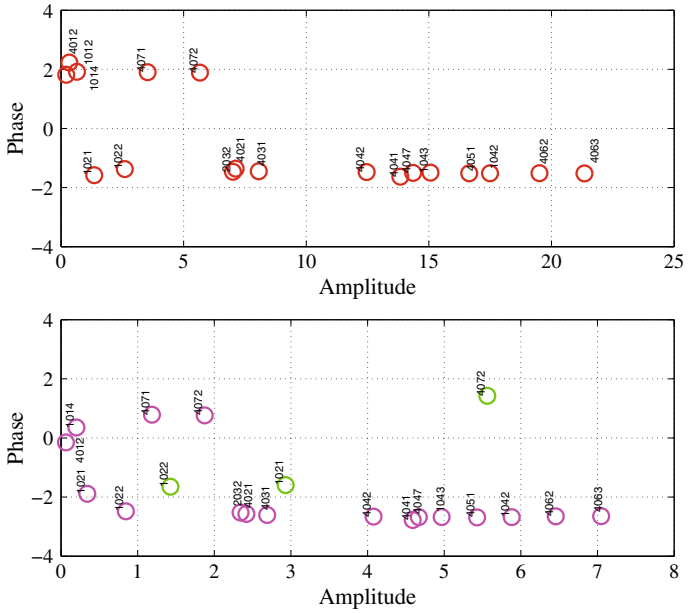

Fig. 9.15 Coherency identification including non-synchronous generation (after fault at bus B_{1012})

Table 9.8 Koopman largest mode variation (fault 4031)

Mode j	Growth rate	Frequency (Hz)	Norm $\|\tilde{v_j}\|$	Case
2	0.99797	0.6165	60.08	BC
5	0.99769	0.6097	54.68	1
2	0.99868	0.6552	13.73	2
8	0.9979	0.6349	16.91	3

9.6 Conclusions and Future Work

The document presents an original contribution to the application of the KMA for the coherency pattern identification of power systems system with a gradual large inclusion of non-synchronous generation.

The application of KMA to the studied power system (Nordic 32 system) showed the variation of the coherent groups through the gradual inclusion of power converters. The results show that if a minor replacement of synchronous machines the coherency is not affected, but after the replacement of the 13% of the power in the system, some significant changes in the coherent groups can be identified.

The coherent groups in one operative area can be altered by the increasing inclusion of non-synchronous generation becoming either groups apart or be more coherent with other groups. A general comment can be made in relation to the fault location

since the coherency phenomena is related to it. After studying several faults incorporating the gradual increasing of full converters. The effect of a fault close to a specific generator in the form of acceleration is propagated, and reflected around the closer generators in the form of synchronizing power. Therefore, with the replacement of synchronous machines (inertia reduction), the coherent groups separate different, as the amplitude coefficient separation in the KM showed.

The applied coherency identification method provides a direct calculation and a powerful graphical visualisation tool for observing the coherent groups/subgroups according to the measurements obtained while the dynamics are changing.

This tool has the potential to be integrated in real-time simulator systems and be improved by a sliding window, which means can be applied in situational awareness alert system or control loops design involved in FRC.

KMA application is concise with the slow coherency theory, however with the reduction of inertia in the system, the fault location change the coherent groups in the system.

Future work requires the addition of PSS to non-synchronous generation and other control loops, e.g. synthetic inertia in order to diminish the oscillations.

Acknowledgements Authors are very grateful to the Dr. Fredrik Raak and Prof. Susuki from Kyoto University for the discussion about the Koopman Mode theory, its computation and suggestions of the document.

References

1. Bjornstedt, J.: Integration of non-synchronous generation—frequency dynamics. PhD thesis (2012)
2. Chamorro, H.R., Ordonez, C.A., Peng, J.C., Ghandhari, M.: Non-synchronous generation impact on power systems coherency. IET Gener. Transm. Distrib. **10**(10), 2443–2453 (2016)
3. Bongiorno, M., Petterson, A.: Development of a method for evaluation of wind turbines ability to fulful Swedish grid codes. Tech. Rep. Elforsk Rapport **09**(25) (2009)
4. Blaabjerg, F., Liserre, M., Ma, K.: Power electronics converters for wind turbine systems. IEEE Trans. Ind. Appl. **48**(2), 708–719 (2012)
5. Hui, J., Jain, P.: Power management and control of a wind energy conversion system (WECS) with a fuzzy logic based maximum power point tracking (MPPT). In: IECON 2012—38th Annual Conference on IEEE Industrial Electronics Society, pp. 5966–5971 (2012)
6. Lalor, G., Mullane, A., OMalley, M.: Frequency control and wind turbine technologies. IEEE Trans. Power Syst. **20**(4), 1905–1913 (2005)
7. Wang, Y., Delille, G., Bayem, H., Guillaud, X., Francois, B.: High wind power penetration in isolated power systems—assessment of wind inertial and primary frequency responses. IEEE Trans. Power Syst. **28**(3), 2412–2420 (2013)
8. Chamorro, H.R., Sanchez, A.C., Overjordet, A., Jimenez, F., Gonzalez-Longatt, F., Sood, V.K.: Distributed synthetic inertia control in power systems. In: 2017 International Conference on Energy and Environment (CIEM), pp. 74–78 (2017)
9. Muljadi, E., Gevorgian, V., Singh, M., Santos, S.: Understanding inertial and frequency response of wind power plants. In: IEEE Power Electronics and Machines in Wind Applications (PEMWA), pp. 1–8 (2012)
10. Brisebois, J., Aubut, N.: Wind farm inertia emulation to fulfill hydro-Quebec specific need. In: IEEE Power and Energy Society General Meeting, pp. 1–7 (2011)

11. Chavez, H., Baldick, R., Sharma, S.: Regulation adequacy analysis under high wind penetration scenarios in ERCOT nodal. IEEE Trans. Sustain. Energy **3**(4), 743–750 (2012)
12. Finley, A., Kosterev, D.: Planning efforts to evaluate dynamic response of increased penetration of variable generation within the western interconnection. In: IEEE Power and Energy Society General Meeting, pp. 1–8 (2012)
13. Gautam, D., Vittal, V., Harbour, T.: Impact of increased penetration of DFIG-based wind turbine generators on transient and small signal stability of power systems. IEEE Trans. Power Syst. **24**(3), 1426–1434 (2009)
14. Chamorro, H.R., Ghandhari, M., Eriksson, R.: Influence of the increasing non-synchronous generation on small signal stability. In: IEEE PES General Meeting|Conference & Exposition, National Harbor, pp. 1–5 (2014)
15. Eftekharnejad, S., Vittal, V., Heydt, G.T., Keel, B., Loehr, J.: Small signal stability assessment of power systems with increased penetration of photovoltaic generation: a case study. IEEE Trans. Sustain. Energy **4**(4), 960–967 (2013)
16. Bueno, P.G., Hernández, J.C., Ruiz-Rodriguez, F.J.: Stability assessment for transmission systems with large utility-scale photovoltaic units. IET Renew. Power Gener. **10**(5), 584–597 (2016)
17. Naik, P., Qureshi, W., Nair, N.-K.: Identification of coherent generator groups in power system networks with wind-farms. In: Universities Power Engineering Conference (AUPEC) pp. 1–5 (2011)
18. Gallai, A., Thomas, R.: Coherency identification for large electric power . IEEE Trans. Circuits Syst. **29**(11), 777–782 (1982)
19. Lee, S.T.Y., Schweppe, F.C.: Distance measures and coherency recognition for transient stability equivalents. IEEE Trans. Power Appar. Syst. **92**(5), 1550–1557 (1973)
20. Podmore, R.: Identification of coherent generators for dynamic equivalents. IEEE Trans. Power Appar. Syst. **97**(4), 1344–1354 (1978)
21. Jonsson, M., Begovic, M., Daalder, J.: A new method suitable for real-time generator coherency determination. IEEE Trans. Power Syst. **19**(3), 1473–1482 (2004)
22. Chow, J., Galarza, R., Accari, P., Price, W.: Inertial and slow coherency aggregation algorithms for power system dynamic model reduction. IEEE Trans. Power Syst. **10**(2), 680–685 (1995)
23. Winkelman, J.R., Chow, J., Bowler, B.C., Avramovic, B., Kokotovic, P.: An analysis of interarea dynamics of multimachine systems. IEEE Trans. Power Appar. Syst. **PAS-100**(2), 754–763 (1981)
24. Agrawal, R., Thukaram, D.: Support vector clustering-based direct coherency identification of generators in a multi-machine power system. IET Gener. Transm. Distrib. **7**(12), 1357–1366 (2013)
25. Djukanovic, M., Sobajic, D.J., Pao, Y.H.: Artificial neural network based identification of dynamic equivalents. Electric Power Syst. Res. **24**(1), 39–48 (1992)
26. Lino, O., Fette, M., Dong, Z., Ramirez, J.: Nonlinear approaches for dynamic equivalencing in power systems. In: Power Systems Conference and Exposition, pp. 1306–1314 (2006)
27. Wang, M.-H., Chang, H.-C.: Novel clustering method for coherency identification using an artificial neural network. IEEE Trans. Power Syst. **9**(4), 2056–2062 (1994)
28. Verma, K., Niazi, K.R.: Generator coherency determination in a smart grid using artificial neural network. In: IEEE Power and Energy Society General Meeting, pp. 1–7 (2012)
29. Tianqi, L., Jun, W., Xuan, L., Xingyuan, L.: A fuzzy clustering method for coherent generator groups identification based on A-K. In: International Conference on Sustainable Power Generation and Supply, 2009. SUPERGEN 09, pp. 1–4, Apr 2009
30. Wang, S.-C., Lee, S.-C., Wu, C.-J.: Analysis of Taiwan power system dynamic performance and coherency identification of synchronous generators using fuzzy c-means clustering. In: Proceedings of SICE Annual Conference (SICE), pp. 1420–1425 (2011)
31. Gil, M., Rios, M., Gomez, O.: Coherency identification based on maximum spanning tree partitioning. In: IEEE PowerTech (POWERTECH), pp. 1–6 (2013)
32. Wei, J., Kundur, D.: A multi-flock approach to rapid dynamic generator coherency identification. In: IEEE Power and Energy Society General Meeting (PES), pp. 1–5 (2013)

33. Avdakovic, S., Becirovic, E., Nuhanovic, A., Kusljugic, M.: Generator coherency using the wavelet phase difference approach. IEEE Trans. Power Syst. **29**(1), 271–278 (2014)
34. Senroy, N.: Generator coherency using the Hilbert Huang transform. IEEE Trans. Power Syst. **23**(4), 1701–1708 (2008)
35. Xu, G., Vittal, V.: Slow coherency based cutset determination algorithm for large power systems. IEEE Trans. Power Syst. **25**(2), 877–884 (2010)
36. Rios, M., Gomez, O.: Identification of coherent groups and PMU placement for inter-area monitoring based on graph theory. In: IEEE PES Conference on Innovative Smart Grid Technologies (ISGT Latin America) pp. 1–7 (2011)
37. Susuki, Y., Mezic, I.: Nonlinear Koopman modes and coherency identification of coupled swing dynamics. IEEE Trans. Power Syst. **26**(4), 1894–1904 (2011)
38. Petersen, K.E.: Ergodic Theory. English, Reprint edition. Cambridge University Press, Cambridge (1989)
39. Lasota, A., Mackey, M.C.: Chaos.: Fractals, and Noise Stochastic Aspects of Dynamics. English, 2nd edn. Springer, New York (1998)
40. Raak, F., Susuki, Y., Hikihara, T., Chamorro, H.R., Ghandhari, M.: Partitioning power grids via nonlinear Koopman mode analysis. In: Innovative Smart Grid Technologies Conference (ISGT), pp. 1–5 (2014)
41. Mezic, I.: Spectral properties of dynamical systems, model reduction and decomposition. Nonlinear Dyn. **41**(1–3), 309–325 (2005)
42. Susuki, Y., Mezic, I.: Nonlinear Koopman modes of coupled swing dynamics and coherency identification. In: IEEE Power and Energy Society General Meeting, pp. 1–8 (2010)
43. Susuki, Y., Mezic, I., Raak, F., Hikihara, T.: Applied Koopman operator for power systems technology. Nonlinear Theory Appl. **7**(4), 430–459 (2016)
44. Bialek, J.: Why has it happened again? Comparison between the UCTE blackout in 2006 and the blackouts of 2003. In: IEEE Power Tech Lausanne, pp. 51–56 (2007)
45. Alsafih, H.A., Dunn, R.: Determination of coherent clusters in a multi-machine power system based on wide-area signal measurements. In: IEEE Power and Energy Society General Meeting, pp. 1–8 (2010)
46. Koch, S., Chatzivasileiadis, S., Vrakopoulou, M., Andersson, G.: Mitigation of cascading failures by real-time controlled islanding and graceful load shedding. In: Bulk Power System Dynamics and Control (iREP)-VI
47. Terzija, V.: Wide area monitoring protection and control—WAMPAC. In: IET-UK International Conference on Information and Communication Technology in Electrical Sciences (ICTES 2007), Dec 2007
48. Moreno, R., Rios, M., Torres, A.: Security schemes of power systems against blackouts. In: 2010 iREP Symposium on Bulk Power System Dynamics and Control (iREP)-VIII (iREP), pp. 1–6, Aug 2010
49. Larsson, S., Ek, E.: The black-out in southern Sweden and eastern Denmark, September 23, 2003. In: IEEE Power Engineering Society General Meeting, vol. 2, pp. 1668–1672, June 2004
50. Norris, S., Shao, H., Bialek, J.: Considering voltage stress in preventive islanding. In: PowerTech (POWERTECH), 2013 IEEE Grenoble, Grenoble, pp. 1–6 (2013)
51. You, H., Vittal, V., Yang, Z.: Self-healing in power systems: an approach using islanding and rate of frequency decline based load shedding. IEEE Trans. Power Syst. **18**(1), 174–181 (2003)
52. Hiyama, T.: Coherency-based identification of optimum site for stabilizer applications. IEE Proc. C (Gener. Transm. Distrib.) **130**(2), 71–74 (1983)
53. Parsa, M., Toyoda, J.: Slow-coherency based composite mode oscillatory stabilization by means of a hybrid PSS. IEEE Trans. Power Syst. **4**(4), 1499–1506 (1989)
54. Zarghami, M., Crow, M., Jagannathan, S.: Nonlinear control of FACTS controllers for damping interarea oscillations in power. IEEE Trans. Power Deliv. **25**(4), 3113–3121 (2010)
55. Chenine, M., Ullberg, J., Nordstrom, L., Wu, Y., Ericsson, G.: A framework for wide-area monitoring and control systems interoperability and cybersecurity. IEEE Trans. Power Deliv. **29**(2), 633–641 (2014)

56. Sun, K., Luo, X., Wong, J.: Early warning of wide-area angular stability problems using synchrophasors. In: IEEE Power and Energy Society General Meeting, pp. 1–6, July 2012
57. Li, W., Bose, A.: A coherency based rescheduling method for dynamic security. IEEE Trans. Power Syst. **13**(3), 810–815 (1998)
58. Diao, R., Vittal, V., Logic, N.: Design of a real-time security assessment tool for situational awareness enhancement in modern power. IEEE Trans. Power Syst. **25**(2), 957–965 (2010)
59. Wang, S., Lu, S., Lin, G., Zhou, N.: Measurement-based coherency identification and aggregation for power systems. In: IEEE Power and Energy Society General Meeting, pp. 1–7, July 2012
60. Nath, R., Lamba, S., Rao, K.S.P.: Coherency based system decomposition into study and external areas using weak coupling. IEEE Trans. Power Appar. Syst. **PAS-104**(6), 1443–1449 (1985)
61. Yusof, S.B., Rogers, G., Alden, R.T.H.: Slow coherency based network partitioning including load. IEEE Trans. Power Syst. **8**(3), 1375–1382 (1993)
62. Tang, K., Venayagamoorthy, G.K.: Online coherency analysis of synchronous generators in a power system. In: 2014 IEEE PES Innovative Smart Grid Technologies Conference (ISGT), pp. 1–5, Feb 2014
63. Stadler, J., Renner, H., Kock, K.: An inter-area oscillation based approach for coherency identification in power systems. In: Power Systems Computation Conference (PSCC), Wroclaw, pp. 1–6 (2014)
64. Padhy, B.P., Srivastava, S.C., Verma, N.K.: A coherency-based approach for signal selection for wide area stabilizing control in power systems. IEEE Syst. J. **7**(4), 807–816 (2013)
65. Susuki, Y., Mezic, I.: Nonlinear Koopman modes and power system stability assessment without models. IEEE Trans. Power Syst. **29**(2), 899–907 (2014)
66. Tu, J.H., Rowley, C.W., Aram, E., Mittal, R.: Koopman spectral analysis of separated flow over a finite-thickness flat plate with elliptical leading edge. In: AIAA Paper 2011, vol. 2864 (2011)
67. Rowley, C.W., Mezic, I., Bagheri, S., Schlatter, P., Henningson, D.S.: Spectral analysis of nonlinear flows. J. Fluid Mech. **641**, 115 (2009)
68. Budiic, M., Mohr, R., Mezic, I.: Applied Koopmanism. Chaos Interdiscip. J. Nonlinear Sci. **22**(4), 047 510 (2012)
69. Force, C.T.: Long term dynamics phase II final report. CIGRE (1995)
70. Chamorro, H.R., Ghandhari, M., Eriksson, R.: Coherent groups identification under high penetration of non-synchronous generation. In: IEEE Power and Energy Society General Meeting (PESGM), pp. 1–5 (2016)